New results from testing relativistic gravity with radio pulsars

Michael Kramer
Max-Planck-Institut für Radioastronomie
Auf dem Hügel 69, 53177 Bonn, Germany
mkramer@mpifr-bonn.mpg.de

We experience a golden era in testing and exploring relativistic gravity. Whether it is results from gravitational wave detectors, satellite or lab experiments, radio astronomy plays an important complementary role. Here one can mention the cosmic microwave background, black hole imaging and, obviously, binary pulsars. This talk will concentrate on the latter and new results from studies of strongly self-gravitating bodies with unrivalled precision. This presentation compares the results to other methods, discusses implications for other areas of relativistic astrophysics and will give an outlook of what we can expect from new instruments in the near future.

Keywords: Pulsars; Neutron stars; Black holes; Gravitational-wave astrophysics; Experimental tests of gravitational theories

PACS numbers: 97.60.Gb; 97.60.Jd; 97.60.Lf; 04.30.Tv; 04.80.Cc

1. Introduction

The latest Marcel-Grossmann Meeting has showed once more that gravity can be explored and tested in many different ways. Whether it is via lab experiments on Earth, in the Solar system or in outer space. Whether it is via radio astronomy, optical/infrared astronomy, high-energy observations or gravitational wave detectors. Nearly all experiments use techniques that were not even remotely thinkable at the time, when Einstein conceived general relativity (GR). And yet, all these experiments that the theory has been confronted with, seem to confirm GR's predictions. Obviously, the phenomena of Dark Matter and Dark Energy, or the incompatibility of GR with quantum physics, justify the search for alternatives and the continuing search for experiments that may eventually show a flaw in Einstein's theory.

In this endeavour it is important to complement the different approaches as they test different regimes of gravity, in each of which one may find a deviation for a given theory. This is illustrated in Figure 1. In the solar systems, gravity tests are made in the quasi-stationary weak-field regime, often involving satellite experiments of high precision (e.g. Ref. 1). The quasi-stationary strong-field regime can be probed with experiments such as stellar orbits around Sgr A* (e.g. Ref. 2) or radio images of black holes (Ref. 3). But also pulsar experiments contribute to this regime, and indeed they already allow precision tests of the radiative properties of gravity (e.g. Ref. 4), as we also show in the following. Using radio pulsars

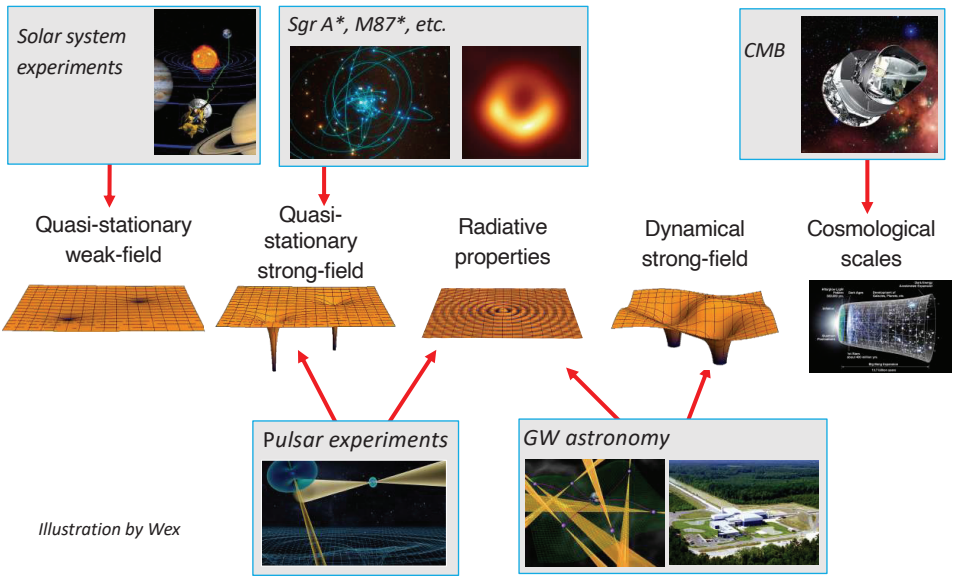

Fig. 1. Different regimes of gravity tests and examples of methods and experiments that allow tests in those.

also as galaxy-sized gravitational wave (GW) detectors (e.g. Refs. 5), one also enters the dynamical strong-field regime, where obviously also the Earth-bound GW detectors are operating (e.g. Ref. 6). Finally, theories should also be tested on the largest scales, which can be done, for instance, with studies of the cosmic microwave background (CMB).

We note that in most of these experimental methods (certainly in those examples given here) radio astronomy plays a crucial role. In the following, we will concentrate on recent results involving radio pulsars.

2. Testing gravity with pulsars

The most common, and most well known way, of testing gravity with pulsars is via a technique called pulsar timing.[7] Less common but still powerful is the usage of pulse structure data that allow us to probe precessional effects when the line-of-sight through the emission beam is changing, modifying the observed pulse properties like width or generally pulse shape.[8] In extreme cases, the pulsar may completely disappear from our view after a while.[9,10])

In pulsar timing one makes use of the often very stable rotation of a pulsar that leads to a regularity in the emitted pulsed signal, caused by a lighthouse effect, that rivals the best atomic clocks on Earth. As an observer on Earth, we can measure the arrival time of the pulses at the telescope and infer from it the motion of the

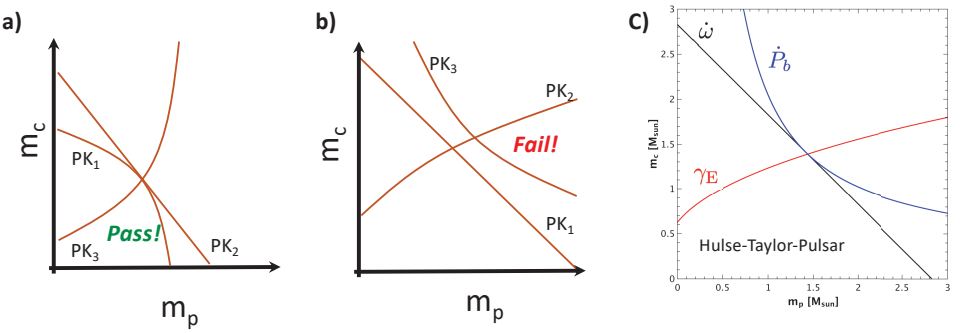

Fig. 2. Gravity tests using binary pulsars performed via the measurements of Post-Keplerian (PK) parameters and their graphical representation in a mass-mass diagram. a) all PK parameter lines insect in a single point: the test is passed. b) the lines do not intersect in a single point: the theory fails the test. c) Example for the Hulse-Taylor pulsar, here shown for general relativity.

pulsar in a binary orbit. The timing precision that is attainable (i.e. better than 100 ns in many cases) is provided by following the rotational phase of the pulsar in a coherent fashion, making measurements more precise as the time baseline increases. In a similar way, tracking the orbital phase reveals periodic and secular deviations from a simple Keplerian orbit, expressed in the so called Post-Keplerian (PK) parameters.[8,11,12] Those can typically be expressed as functions of the Keplerian parameters and the two unknown masses of the binary system. Once two PK parameters can be measured, the two masses can be determined within the framework of a given theory and the value of further PK parameters can be predicted. Once that is done, the predictions can be compared with similar measurements and the theory, hence, can be tested.

One can express such a test in a graphical form, where each PK parameter describes a line in a diagram with the values of two unknown masses as its axes. Two PK parameter lines define an intersection point through which every other PK parameter line must pass. If that is not the case, the theory determining the lines is falsified and needs to be rejected. The measurement uncertainties in the PK parameters is expressed as the width of the PK lines in the mass-mass diagram. See Figure 2.

2.1. *The Double Pulsar*

We demonstrate the power of pulsar timing using the best laboratory currently known, the so called "Double Puslar".[13,14] The system consists of two active radio pulsars – a currently still unique feature of the system – orbiting each other in 147 min. The recycled (old) pulsar (A) in the system has a period of 23 ms, the non-recycled (young) pulsar (B) a period of 2.8 s. An important feature of the system is its edge-on geometry (see Figure 3) that also leads to 30-s long eclipses and our

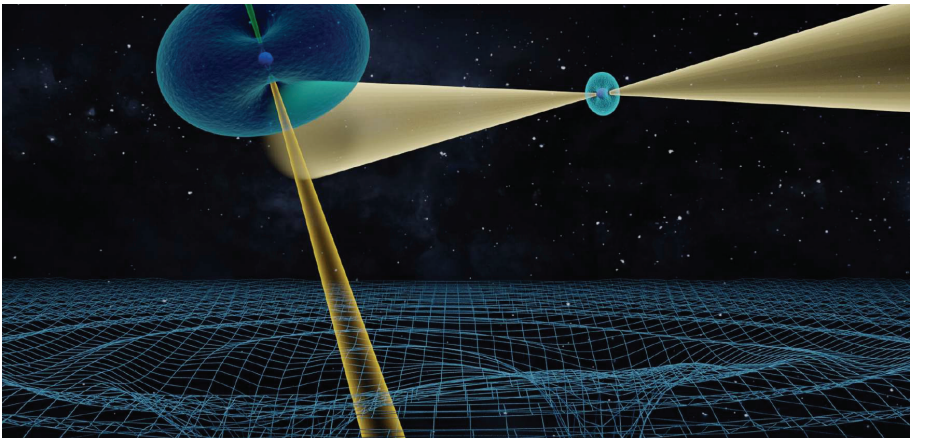

Fig. 3. Artistic impression of the Double Pulsar. Here, two active radio pulsars orbit each other in 147 min in a slightly eccentric orbit ($e = 0.09$). One pulsar is old and recycled ($P = 23$ ms), while the second pulsar is young ($P = 2.8$ s). Figure is not to scale.

ability to measure light-propagation effects (see below). The previous gravity tests with the system made usage of the ratio of the masses of the two pulsars, that can be directly (i.e. theory independently to 1PN order) measured from the two semi-major axes the pulsars' orbit around the common centre of mass.[4] Meanwhile the data have improved very significantly in both precision and length. The latest results were presented by Kramer et al. (Ref. 15), reporting the measurement of, in total, seven PK parameters.

What is important and different to previous experiments, the measurement precision is now so high that for the first time higher-order contributions need to be taken into account for some of the PK parameters. This includes the contribution of the A pulsar's effective mass loss (due to spin-down) to the observed orbital period decay, a relativistic deformation of the orbit, and the effects of the equation of state of super-dense matter on some of the observed PK parameters via relativistic spin-orbit coupling. The system also provides the currently most precise test of general relativity's quadrupolar description of GWs, validating GR's prediction at a level of 1.3×10^{-4} with 95% confidence.[15] As indicated, the impact of the mass loss due to rotational spin-down is taken into account in this result. Interestingly, as the pulsar is losing rotational energy, and while $E = m\,c^2$, the slow-down corresponds to a mass loss of 8.4 Million tons per second or 3.2×10^{-21} of the mass of A per second.

2.1.1. *Light propagation*

The edge-on geometry of the system allows not only a test of relativistic spin-precession as discussed in Section 3, but it also leads to a "Shapiro-delay", i.e. the a delay in the measured arrival time as the photons have to propagate in the curved

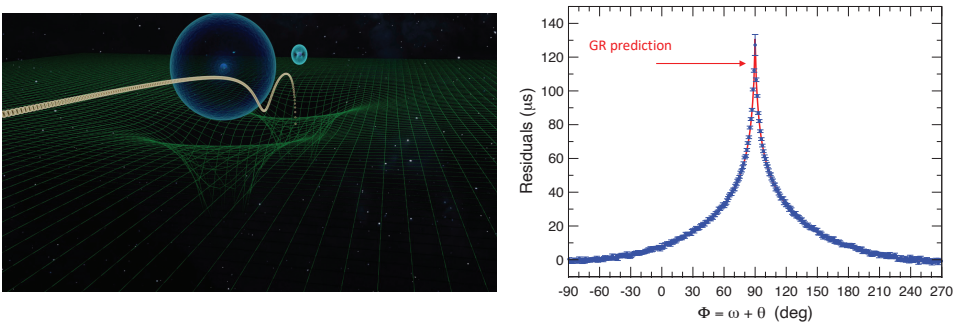

Fig. 4. Shapiro delay measurement in the Double Pulsar. The curvature of spacetime around the companion B (see artistic impression on the left, not to scale) leads to a delay in the arrival times of the pulses of pulsar A (right).

spacetime near the companion pulsar. We illustrate this effect in Figure 4. The data points follow the prediction of GR (red line) remarkable well (at a level of 4×10^{-4} with 95% confidence.[15] This agreement with the data is, however, only achieved when next-to-leading order effects are taking into account: at the 1.5PN limit one has to take into account that the speed of light is finite and that pulsar B moves during the flight time of the photos across the orbit. See Figure 5.

When comparing the Shapiro delay curve with precision data, another effect needs to be considered which relates to the fact the pulsar is indeed a lighthouse rather than a pulsating or oscillating object. This effect is aberration, which for pulsar timing means in principle a delay in arrival time that depends on orbital phase and on the orientation of the pulsar with respect to the orbit and the observer.[12,16] Due to the geometry of the Double Pulsar that does, however, not lead to separately measurable, additional PK parameters.[15] Nevertheless and most interestingly, given the precision obtained in the measurements, the curved spacetime encountered by the photons near superior conjunction leads to a deflection of the signal in the gravitational field of pulsar B. This gravitational signal deflection leads to a small change in the proper angle of emission, which in turn leads to a lensing correction to the classical ("longitudinal") aberration. See Ref. 15 for details. As a result, only those photons reach the observer on Earth that are emitted slightly earlier (or later, respectively) in pulsar rotational phase, before (and after, respectively) superior conjunction. The measurement shown in Figure 6 not only demonstrates the lighthouse character of pulsars but also indicates a prograde alignment of the pulsar spin relative to the total angular momentum vector.

2.1.2. *Orbital deformation, lense-thirring effect and moment-of-inertia*

A further effect that is observed in the Double Pulsar and that is now required to be considered in the data analysis is a relativistic deformation of the orbit. The presence of the effect[11,12] was already seen by Weisberg & Huang (Ref. 17). In

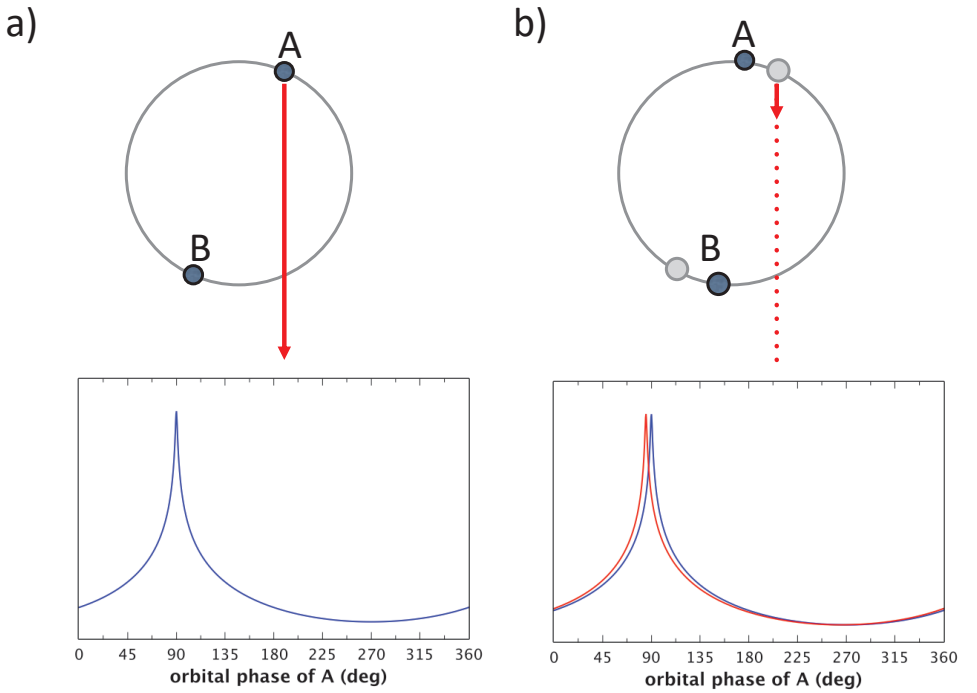

Fig. 5. Illustration of the physical origin and impact of the next-to-leading order (1.5PN) contribution to the Shapiro delay. a) Previously, a "static" Shapiro delay was implemented in timing formula, assuming the position of the companion pulsar B to be fixed during the propagation of A's photons. b) In reality, pulsar B moves during the flight time of the photons, which effectively leads to a small shift in the Shapiro delay curve at the 1.5PN level. Illustration by N. Wex.

this case, ignoring this subtle effect would (wrongly) suggest a tension between the measured "Einstein delay" and its prediction by GR. See Kramer et al. (Ref. 15) for details.

As already indicated, the extreme precision of the experiment now also needs to incooperate the effects of the equation of state (EoS) of super-dense matter on some of the observed post-Keplerian parameters via relativistic spin-orbit coupling. Indeed, the most precisely measured PK parameter, $\dot{\omega}$, representing the precession of the orbit, has a contribution from the Lense-Thirring effect due to the rotation of pulsar A at the 2PN level, which is more than 30 times larger than our measurement error. However, a calculation of the Lense-Thirring contribution requires the knowledge of the Moment-of-Inertia of pulsar A, $I_{\rm A}$, which comes with a significant uncertainty due to our imperfect knowledge of the EoS for neutron star matter. To constrain $I_{\rm A}$ one can use constraints on the EoS obtained from the double neutron star merger GW170817[18] and determine precise measurements for the pulsars. Alternatively, one can ignore any existing constraints on the EoS of neutrons stars to simultaneously determine the pulsar masses, $m_{\rm A}$, $m_{\rm B}$, and $I_{\rm A}$, assuming GR to be

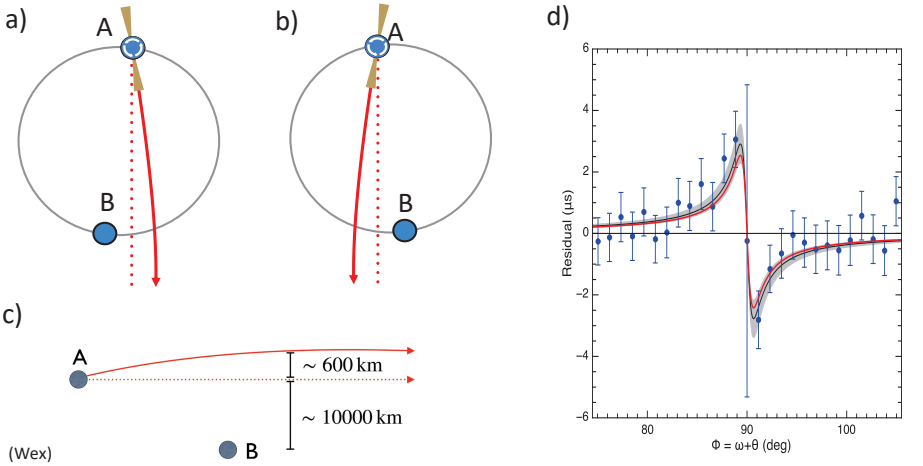

Fig. 6. Illustration and measurement of another next-to-leading order effect that needs to be taken into account for the Shapiro delay. In this case, aberrational light bending due to the curvature of spacetime around pulsar B is considered. a) Before superior conjunction, the photons have to be emitted at a slightly later rotational phase than usual to compensate for the light bending near B to reach the observer on Earth. b) After superior conjunction, the photons have to be emitted slightly earlier, respectively. c) The light bending contributes an additional 600 km to the total impact distance. d) Residuals observed near superior conjunction (i.e. periastron, $\Phi = 0$ deg), when this effect is *not* taken into account. The red curve shows the theoretical prediction arising from this effect, and the black curve corresponds to the best fit, with a 2σ range indicated by the light grey band. This effect allows us to infer the spin direction of pulsar A, indicating a prograde orientation. See Kramer et al. (2021) for details.

the correct theory of gravity. In this case, simply based on pulsar timing, one finds for the the MoI $I_{\rm A} < 3.0 \times 10^{45}\,{\rm g\,cm^2}$ with 90% confidence,[15] which in turn can be directly compared to the results derived from the GW170817 LIGO/Virgo merger and from NICER X-ray timing. Using a universal relation, like the one in Ref. 19, one can convert the obtained probability distribution of $I_{\rm A}$ into a probability distribution for A's radius. With 90% confidence, this gives an upper limit for A's radius of 22 km, a value outside any physically valid EoS but purely based on the arrival times measurements of pulses.[15]

In summary, the Double Pulsar allows to test conservative aspects of the orbital dynamics of two strongly self-gravitating masses up to 2PN order, including a $\sim 1\sigma$ constraint on the Lense-Thirring contribution, which in turn can be used to constrain the MoI of pulsar A under the assumption of GR. The experiments allow to test the propagation of photons in the gravitational field of a strongly self-gravitating (material) body, with next-to-leading-order contributions being clearly present in the timing data, confirmed with a precision of about 10%. We can also test the radiative aspects of GR, yielding a test at 2.5PN level in the equations of motion with a precision of 1.3×10^{-4} (95% C.L.). In terms of overall fractional precision, this is the most precise test of GR's predictions for GW emission

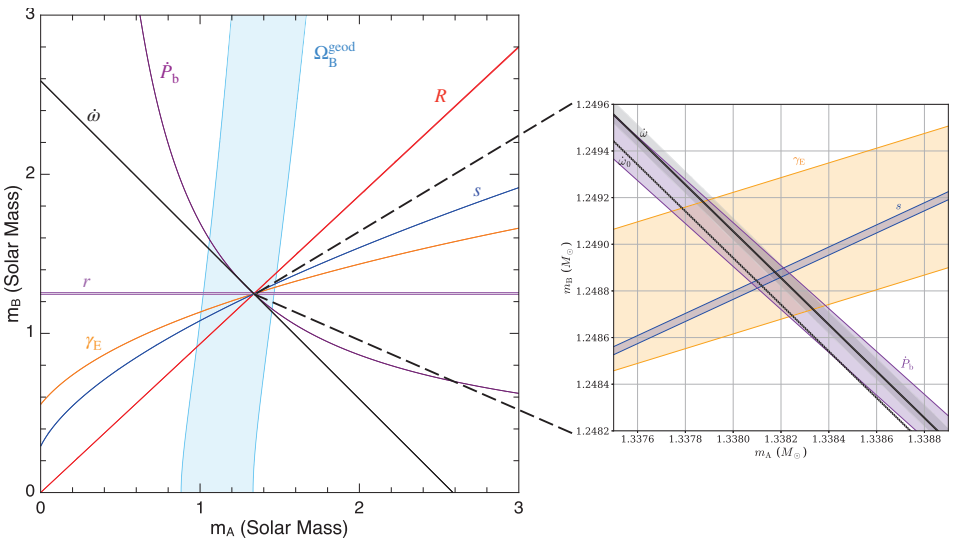

Fig. 7. Mass-mass diagram for the Double Pulsar as presented by Kramer et al. (2021). The right panel is a zoomed-in version of the intersection point of the PK parameter lines in the left panel. The shift of the line for the PK-parameter $\dot{\omega}$ when ignoring the Lense-Thirring effect ($\dot{\omega}_0$) is clearly visible. See text for details.

currently available. These tests are summarized in the mass-mass diagram shown in Figure 7.

3. Relativistic spin-precession

A gyroscope freely falling in curved spacetime suffers a precession with respect to a distant observer. Experiments made in Solar System provide precise weak-field tests and confirm it, e.g. with Lunar Laser Raning or GRAVITY Probe-B. In a binary pulsar system, the pulsar - also being a gyroscope - we observe, strictly speaking, a mixture of different contributions to relativistic spin-orbit coupling. One contribution comes from the motion of the first body around the centre of mass of the system (deSitter-Fokker precession), while the other comes from the dragging of the internal frame at internal frame at the first body due to the translational motion of the companion.[20] This resulting relativistic spin-precession causes nevertheless the expected effect: the pulsar precesses about the total angular momentum, which as a result changes the relative orientation of the pulsar towards Earth with potentially observable consequences as predicted by Damour & Ruffini in Ref. 21 even before the publication of the discovery of the Hulse-Taylor binary pulsar.[22] We note that the orbital angular momentum is expected to be much larger than that of a pulsar in the system, so that the orbital spin practically represents a fixed direction in space. Hence, effectively the pulsar precesses about the orbital angular momentum.

The precession rate, $\Omega_{\rm SO}$, is another PK as introduced above. Assuming GR to be valid, it is given by[23]

$$\Omega_{\rm SO} = T_\odot^{2/3} \left(\frac{2\pi}{P_{\rm b}}\right)^{5/3} \frac{m_{\rm A}(4m_{\rm B}+3m_{\rm A})}{2(m_{\rm B}+m_{\rm A})^{4/3}} \frac{1}{1-e^2}. \quad (1)$$

The effect of relativistic sin precession on pulsar timing is in principle measurable due to a change in the aberration parameters with time.[8] Much more obvious, and hence easier to measure, are the consequences of the changing line-of-sight as the pulsar precesses. We expect changes in the pulse shape (e.g. in simply the measured width, but also more dramatic changes) and especially in the measured linearly polarised emission which is a sensitive probe of the pulsar geometry.[21,24] Such measurements have indeed enabled the detection of spin precession in a number of relativistic binaries. After the first detection in the Hulse-Taylor pulsar B1913+16[9,25] and later in PSR B1534+12,[26,27] it is now possible to convert long-term observations in precise quantitative tests of spin precession and, hence, test of the "effacement" property of a spinning body.

3.1. *Spin precession in the Double Pulsar*

A prime example to study relativistic spin precession is, again, the Double Pulsar. Here, we have two active pulsars, both of which could, in principle show the effects of precession. However, it turns out that the supernova explosion creating the second-born pulsar, B, was a low-kick supernova which left the pre-Supernova orientation of the orbital angular momentum vector unchanged. The spin of pulsar A, having been aligned with the orbital spin during its recycling period, is therefore still aligned with it, so that precession for A is not expected. Indeed, so far, profile changes for A have not been detected, suggesting that A's misalignment angle is less than 3 deg.[28,29]

In contrast, secular changes in the pulse shape and the orbital visibility windows of pulsar B were observed soon after its discovery,[30] providing early evidence for spin precession of B. Around 2008, the pulsar vanished from our view when our line-of-sight moved out of the emission beam.[10] B will eventually re-appear. The exact epoch for this to happen depends on the actual beam shape, but despite a precession period of 71 years (see Table 1), it could happen relatively soon.[10,31]

Meanwhile, it has been possible to track the orientation of the spin axis of pulsar B in a rather fortuitous way: Breton et al. (Ref. 32) studied the time evolution of the $\sim$ 30-s long eclipses of A that are caused by the blocking rotating magnetosphere of B at superior conjunction. This absorption of the background emission, presumably by synchrotron self-absorption,[33] is not complete, but because of the torus-shaped dipolar magnetosphere[a] the light from the background pulsar A is visible every half-turn or full-turn of pulsar B, depending on the orientation of the spin-axis and,

[a]Deviations from a purely dipolar-shaped magnetosphere do exist and are observed. Indeed, about 50% of the magnetosphere is "missing" but for the remaining parts, the torus shape appears more than adequate, as the successful modelling shows. See, for instance Ref. 34.

hence, the magnetosphere. Applying a simple but successful geometrical model,[33] Breton et al. were able to explain the observed modulation of A's lightcurve during the eclipse phase in great detail. Model-fitting indicates a constant magnetic inclination angle and constant misalignment angle, while the azimuthal spin angle is changing with a rate of $\Omega_{\rm SO,B} = 4.77^{+0.66}_{-0.65}{}^{\circ}$ yr^{-1}, in agreement with general relativity[32] (see Table 1).

3.2. *PSR J1906+0746 – The currently best test*

A further observational consequence of relativistic spin precession is its impact on the polarisation properties of binary pulsars. Here, two separate but related aspects are observable.

The first aspect is due to the changing line-of-sight within the pulsar beam. According to the rotating vector model (RVM),[24] we expect an S-like swing of the position angle of the linearly polarised emission component of the studied pulsar. The closer the line-of-sight approaches the magnetic axis, the steeper is the expected S-swing. In general, the shape of the S-swing depends on four quantities: the magnetic inclination angle, α, between the spin and magnetic axes, the impact angle between our line-of-sight and the magnetic axis, β, the pulse phase, ϕ, and, finally, the absolute (reference) position angle, Ψ_0, which is obtained at $\phi = 0$ and identical to the orientation of the pulsar spin-axis projected on the plane of the sky. Such a measurement was first achieved for PSR B1534+12,[26,27] where the impact angle β was observed to change with time.

The second consequence is the change of Ψ_0 due to the changing orientation of the pulsar spin and the resulting projection on the sky.[35] This change of the absolute position angle is periodic, with a period equal to the precessional period. Note that there is also a small contribution due to orbital aberration, which we will ignore here. We note that the measured absolute position angle will be affected by Faraday rotation due to propagation in the magnetised ionised interstellar medium. But this effect can, in principle, be measured and removed.

It is the additional information provided by the change in absolute position angle that allows to break some degeneracies and to potentially determine the true orbital inclination angle, i (rather than $180-i$, as pulsar timing only provides $\sin i$). Modelling the evolution of the position angle swing in the described way requires in total only four free parameters, i.e. the precession rate, $\Omega_{\rm SO}$, the misalignment angle between pulsar spin and total angular momentum vector, δ, the precession reference phase, $\Phi^0_{\rm SO}$, and the magnetic inclination angle of the pulsar, α. A requirement for precession to occur is $\delta > 0$, a measurement of which is very useful to study the formation of the system (see Refs. 34 and 35 for a detailed discussion on this topic).

Both aspects just described are relevant for the beautiful case of PSR J1906+0746. This pulsar is an almost perfect orthogonal rotator, and so this pulsar was discovered with the emission from both magnetic poles being visible

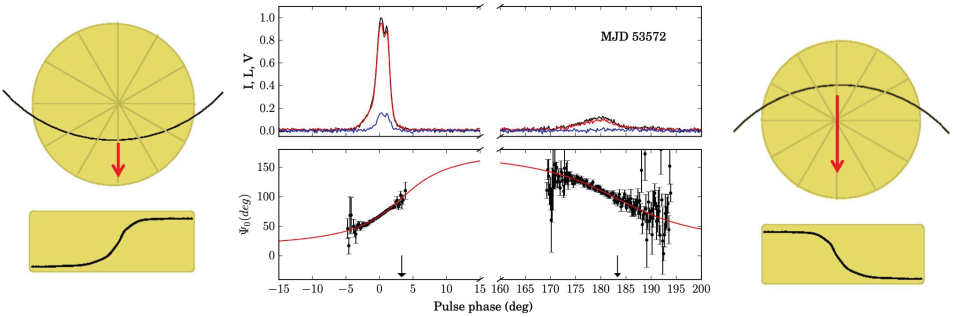

Fig. 8. Pulse profile of PSR J1906+0746 as observed by Desvignes et al. (2019) shown in the middle panel. Both magnetic poles (schematics left and right) were originally visible after discovery. Their observed emission is highly linearly polarised (red line), with a position angle swing (middle lower panel) that resembles a textbook-like rotating vector model. The pulsar also shows a modest amount of circularly polarised emission (middle upper panel, blue line). At the left pole, our line-of-sight moves out of the beam, while at the right pole our line-of-sight crossed the magnetic pole during the long-term monitoring of this source.

(see Figure 8). The emission's high degree of linear polarisation reveals a perfect RVM-like behaviour of the measured position angle that was studied by Desvignes et al. (Ref. 36). Fitting those to the RVM as a function of time using the precessional RVM model[35] described above, allows to measure the precession rate to $\Omega_{\rm SO} = 2.17 \pm 0.11$ deg/yr which is in perfect agreement with the expectation from GR (see Table 1). This test is the currently best test of relativistic spin-precession for strongly self-gravitating bodies.

The study of the position angle reveals even more: Apart from providing measurements of the geometry of the system ($i = 45 \pm 3$ deg, $\alpha = 99.4 \pm 0.2$ deg, $\delta = 104 \pm 9$ deg), the evolution of the position angle swing with time shows how its slope becomes steeper when our lines-of-sight approaches the magnetic pole. It also shows how it swaps sign in slope when crossing the pole, and how it becomes flatter again when moving away from the pole[36] (see right of Figure 9). This is the first unequivocal evidence that the RVM is correct and that the position angle swing of pulsars is in principle determined by the geometry of the pulsar and its fieldlines. Deviation may, however, still occur in cases due to propagation effects or modifications to the field line structure in the emission region.

Furthermore, we can reconstruct the emission beams of the pulsar as projected on the sky and as shown in the left two panels of Figure 9). As the light of sight crosses the two beams, we can obtain "tomographic" images, albeit incomplete ones due to lack of observations in part of the beam. We note from the middle panel, showing the pole that is responsible for the (initially) weaker pulse component in Figure 8, that the emission beam is active on either side of the pole, ruling out models that predict radio emission to be restricted to one side of the pole. Secondly, the emission pattern is not symmetric in the latitudinal direction relative

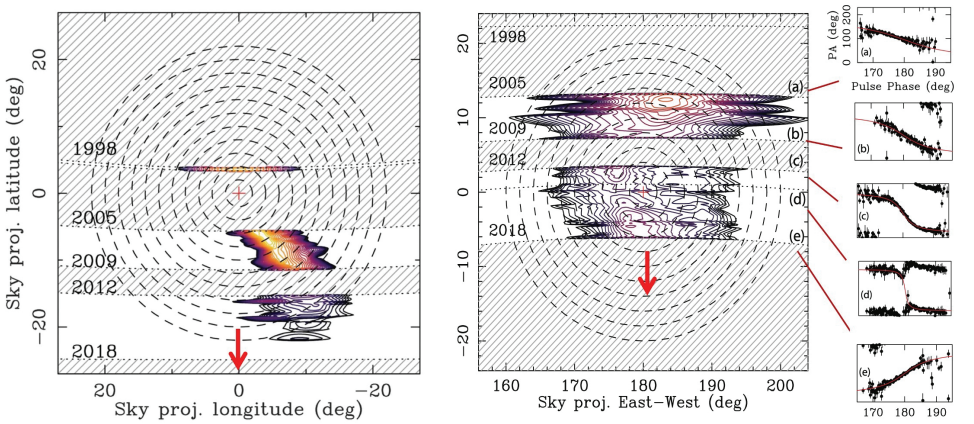

Fig. 9. Beam pattern of the two magnetic poles of PSR J1906+0746 as projected on the sky and observed by Desvignes et al.[36] The beams are reconstructed from observations spanning more than 10 years, when our line-of-sight moved in the indicated direction above both poles. For the right beam, our line-of-sight crossed the magnetic pole. The resulting position angle swing shown on the right evolves with time as expected from the rotating vector model (see text for details). For the left beam, the emission becomes weaker to the beam edge and the initially much stronger component (see Figure 8) is hardly detectable anymore and will soon vanish completely.

to the pole. When looking more closely at our data, we also notice that above the pole itself the emission is reduced, matching theoretical predictions for the current density in the polar cap for an orthogonal rotator.[37] What is also not visible in these total intensity plots shown here (see Ref. 36 for details) is an interesting behaviour of the polarisation characteristics more generally: the handedness of the circularly polarised emission changes when crossing the pole, the fractional linear polarization overall decreases with increasing distance to the beam centre, and finally, emission heights inferred from polarisation data increase from very low emission heights near the pole to emission heights of several hundreds of kilometres at the beam edge, again consistent with theoretical expectations[38] and inferred more indirectly from other pulsars.[39,40]

In summary, somewhat unexpectedly, an experiment designed to test theories of gravity and to tests predictions made by Thibault Damour and Remo Ruffini nearly 50 years ago, leads to unique insight into the emission physics of pulsars.

3.3. *Relativistic spin precession in other pulsars*

Today, spin precession has been routinely observed in all those binary pulsars, where we can expect the pulsar spin to be misaligned with the orbital momentum vector (i.e. systems where we observe the young pulsar or where the last supernova explosion in the system imparted a large kick onto the newly born neutron star) and where the precession rate is high enough due to a sufficient compactness of the orbit. Using the precession rate as given in GR, Eqn. 1, we provide a list of pulsars

where we would expect to observe spin precession. Table 1 gives the corresponding values, sorted by decreasing rate. We note that for the vast majority of sources, spin precession has been detected (see Ref 41). The second highest rate is expected for the highly accelerated binary pulsar J1757−1854 discovered with in the High Time Resolution Universe Survey.[42] As presented by Cameron et al. in this conference, first signs of profile changes may already be present but further data are needed. If this is confirmed, the first top-6 pulsars (and seven out of eight) have all been observed to undergo spin precession. The only other exception in the table is PSR J1756−2251. Here the spin may be aligned with the orbital momentum vector, but studies are in progress to revisit this pulsar with larger precision and longer time baseline.[43]

Table 1. Binary pulsar systems where relativistic spin precession is expected or observed, ordered according to the precession rate as expected from general relativity. Pulsars marked with an asterisk have been identified of showing spin precession.

PSR	P(ms)	$P_{\rm b}$ (d)	x(lt-s)	e	$\Omega_{\rm p}$ (deg yr^{-1})
J0737−3039A/B*	22.7/2770	0.10	1.42/1.51	0.09	4.8/5.1
J1757−1854	22.50	0.18	2.24	0.61	3.1
J1906+0746*	144.1	0.17	1.42	0.09	2.2
B2127+11C*	30.5	0.34	2.52	0.68	1.9
J1141−6545*	394.0	0.20	1.89	0.17	1.4
B1913+16*	59.0	0.33	2.34	0.62	1.2
J1756−2251	28.5	0.32	2.76	0.18	0.8
B1534+12*	37.9	0.42	3.73	0.27	0.5

4. Further recent tests with radio pulsars

In this work, we have so far concentrated on a few prominent, perhaps even spectacular recent examples of using pulsars for testing strong-field gravity. Much more can be studied, including fundamental concepts, such as the Universality of Free Fall (UFF) and the Strong Equivalence Principle (SEP), the possible variation of fundamental constants, or bounds on the graviton mass. We can also test specific alternatives to GR. Here, we refer to recent reviews (see Refs. 44, 45 for more in-depth discussions) and we point to other contributions of the MG16 meeting. Here, we will only highlight some recent examples.

4.1. *Universality of Free Fall (UFF)*

The UFF can be tested in the various regime that we discussed in context of Figure 1. In the solar system, we refer to the superb measurement using test masses aboard the MICROSCOPE satellite that was launched in April 2016 and operated until October 2018. The results indicate that any violation of the weak equivalence principle, Δ, is smaller than $\Delta < 10^{-15}$ (see Ref. 1).

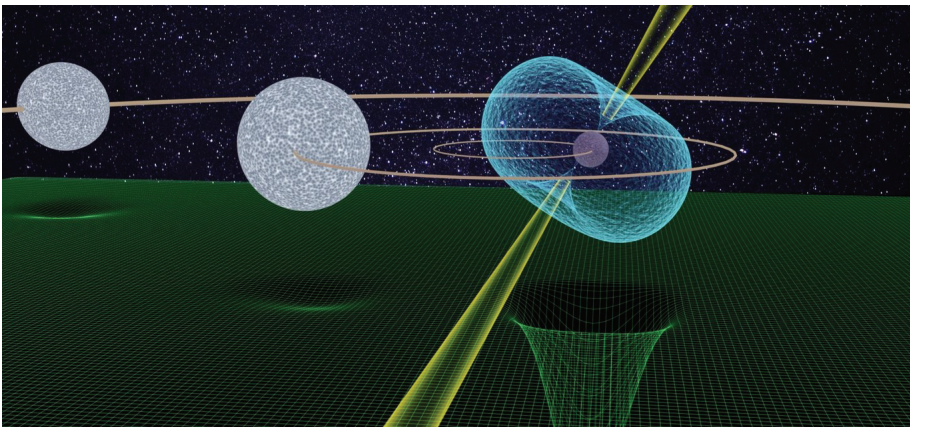

Fig. 10. Artistic impression of the Triple System, where a 2.7-ms pulsar, PSR J0337+1715, and a $0.20 M_\odot$ white dwarf are in an inner 1.63-day orbit, while being orbited themselves by a second $0.41 M_\odot$ white dwarf in 327 days. The figure is not to scale.

The Earth-Moon system allows to test the fall of two bodies with different gravitational self-energy, $\epsilon = E_{\rm grav}/mc^2$, where $E_{\rm grav}$ is the Newtonian gravitational binding energy, in the gravitational field of the Sun. For the Earth $\epsilon_E = -4.6 \times 10^{-10}$ and for the Moon, $\epsilon_M = -0.2 \times 10^{-10}$. The fall can be measured with Lunar Laser Ranging and limits on a deviation are currently at $\Delta < 2 \times 10^{-13}$.[46,47] Comparing this to the gravitational self-energy of the involved bodies, a limit on the violation of the SEP in the weak field of the solar system is $\Delta/\epsilon < 0.04\%$.

Pulsars allow us to test the SEP for strongly-self gravitating bodies, i.e. $\epsilon = -0.13$. The idea was already presented by Damour & Schäfer in 1991 (Ref. 48) who proposed to study the possible variation of the orbits of pulsar-white dwarf systems as they fall in the gravitational potential of the Milky Way. The discovery of a Triple System,[49] a pulsar with two White Dwarf (WD) companions, allows an important variation of this experiment, leading to a much more stringent test (see Figure 10).

The 2.7-ms pulsar, also known as PSR J0377+1715 is in a 1.63-day orbit with a WD of mass $0.2 M_\odot$. This inner binary system is orbited by a second, more massive WD ($0.41 M_\odot$) in a 327-day orbit. As pointed out already by Freire et al. (Ref. 50), in such a case, the pair of bodies with different gravitational self-energy falls in the gravitational potential of the outer WD, providing a much stronger field than that of the Milky Way. Archibald et al. (Ref. 51) presented the result of such an experiment and derived a limit of $\Delta < 2 \times 10^{-6}$. This may appear weaker than the weak-field limit from the solar system, but the SEP should apply for both weak- and strong-field conditions. Hence, when referring to a corresponding $\Delta/\epsilon < 0.002\%$, the importance of this measurement becomes clear.

Even more recently, Voisin et al. (Ref. 52) presented an important improvement on the experiment, using a completely independent data set. The improvements arise from a more uniformly sampled data set but also from an improved theoretical

treatment that incorporates the interesting parameter Δ directly into the analysis of the timing data set. The result is a limit of $\Delta = (+0.5 \pm 1.8) \times 10^{-6}$ at 95% confidence level. While the numerical improvement upon Ref. 51 is 30%, this result is statistics-limited and avoids limitation by systematics as previously encountered.

We complete this section by also referring to recent results and proposals for further experiments to test the UFF also towards dark matter. See Ref. 53 for more details.

4.2. *Alternative theories of gravity*

Despite the successes of GR when being confronted with experimental data, GR may not be our final answer in describing gravity on a macroscopic scale. Given a number of unsolved questions (e.g. dark matter, dark energy, inflation) or its incompatibility with quantum mechanics, is still possible that we encounter an experiment that contradicts GR's predictions. In this case, we would learn important and substantial lessons, and so it is important to explore all regimes presented in Figure 1, probing different aspects of the predictions of GR and alternative theories with different methods. For instance, observations with GW detectors are able to test the highly dynamical strong-field regime and radiative aspects of gravity, but they are not able to test aspects of light-propagation in strong fields. This may be eventually possible with images from super-massive black holes, but the curvature of spacetime is many orders of magnitude smaller than around stellar compact objects. This, on the other hand, and other aspects can be tested with binary pulsars.

The close agreement of the Double Pulsar experiment with the predictions of GR shown in Section 2.1 allows us to place tight constraints on various alternatives to GR. Kramer et al. (Ref. 15) used their recent results to study both "Damour–Esposito-Farése" (DEF) gravity and Bekenstein's tensor-vector-scalar theory (TeVeS).[54] The latter is a MONDian relativistic gravity theory that evades the need for dark matter in galaxies by a modification of GR. Even though this theory has been ruled out already with observations of GWs,[55] Ref. 15 points out that pulsar experiments are still useful to test the aspects of scalar field in the theory.

DEF is a two-parameter mono-scalar-tensor gravity,[56] containing GR as a limit with the two parameters $\alpha_0 = \beta_0 = 0$. As other alternative of GR, DEF violates the SEP, which should result in observable dipolar GWs and a location-dependent gravitational constant. We would measure such phenomena in the form of different functional dependencies of the PK parameters as described in Section 2 (see e.g. Ref. 57). Moreover, in certain regions of the parameter space, DEF gravity shows genuine non-perturbative strong-field effects that are only present in NSs and therefore are not testable in the weak-field regime of the solar system. Hence, one can convert our observational results into constraints for the parameters α_0–β_0. This is done by Ref. 15 as shown in Figure 11. It demonstrates that pulsar tests are complementary to each other as well as to other methods.

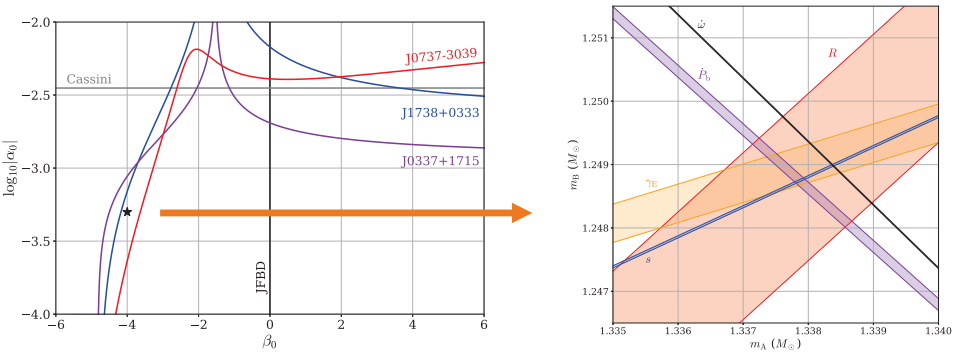

Fig. 11. (Left) Diagram displaying the α_0–β_0 parameter space of DEF gravity. Different experiments provide constraints shown as lines. Parameter space above a line is ruled out. In addition to constraints from the Cassini spacecraft, the figure includes constraints from limits on the existence of dipolar GW emission obtained from PSR J1738+0333, and constraints from the Triple System and the Double Pulsar as described earlier. GR is contained in this parameter space at $(\alpha_0 = 0, \beta_0 = 0)$. The Jordan-Fierz-Brans-Dicke (JFBD) theory is also contained along the vertical $(\beta_0 = 0)$-line. (Right) Every point in the left parameter space corresponds to a specific DEF theory and different realisations of the PK parameters. For a specific choice as an example, indicated by the star in the left figure, one obtains a mass-mass diagram that can be compared to Figure 7. Here, the PK lines fail to intersect in a single point and the specific theory should be rejected. This is already visible by the star's position in the left diagram, left and above the Double Pulsar line. This specific theory, however, would have passed other existing constraints as indicated. See Kramer et al. (2021) for details and references therein.

5. Conclusions

In this contribution, I have tried to summarise some recent key results in probing strong-field gravity using pulsars. In the past three years, the results have not only improved dramatically in precision, but also new effects could be studied. Pulsar continue to play an important role and complement other experiments which have only become possible in the recent years. This includes terrestrial GW detection as well as the imaging of black holes. What is unique about pulsars is the incredible precision that we can obtain in pulsar timing experiments. This is perhaps best demonstrated by the fact that we now have to consider the mass loss of a pulsar spinning down and the interior structure of neutron stars when we one to interpret our results.

Figure 12 attempts to bring the pulsar experiments into context with others. The chosen parameters plotted are a deliberate choice, as they clearly demonstrate that pulsars probe strong-field gravity, as pointed out by many authors in the past (e.g. Ref. 58). It also shows the size of the parameter space to be probed. Future telescopes, like the Square Kilometre Array (SKA), will contribute many more experiments and exciting constraints, as first results with MeerKAT clearly demonstrate.[43] The best is still to come.

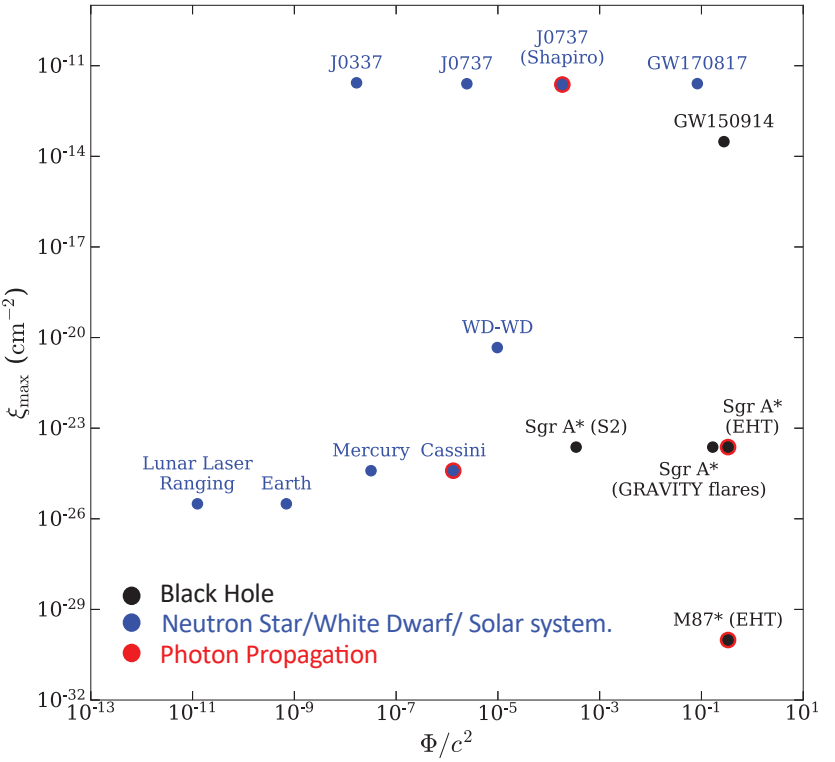

Fig. 12. Parameter space to compare different gravity experiments. While several possible combinations for 2-D diagrams are possible, none is complete in capturing all quantities relevant for gravity tests, and therefore each of them always gives an incomplete comparison. Adopting the plot from Kramer et al. (2021), we show the gravitational potential and the maximum spacetime curvature in a system, distinguishing between weakly and strongly self-gravitating masses amongst material bodies. Experiments that directly probe the coupling between gravitational and electromagnetic fields, i.e. the propagation of photons in a curved spacetime, are highlighted by red circles. We also mark experiments involving black holes as black dots. See Kramer et al. for a discussion of the choice of parameters and further details.

Acknowledgments

I am grateful to the organisers for inviting me to give the presentation. I thank my co-authors in the recent Double Pulsar work and in particular Norbert Wex for providing figures.

References

1. P. Touboul, G. Métris, M. Rodrigues, Y. André, Q. Baghi, et al. *Phys. Rev. Lett.* **119** (December 2017) 231101.
2. Gravity Collaboration,, *A&A* **615** (July 2018) L15.
3. Event Horizon Telescope Collaboration,, *ApJ* **875** (April 2019) L1.

4. M. Kramer, I. H. Stairs, R. N. Manchester, M. A. McLaughlin, A. G. Lyne, et al., R. D., *Science* **314** (2006) 97.
5. S. Chen, R. N. Caballero, Y. J. Guo, A. Chalumeau, K. Liu, et al., *MNRAS* **508** (December 2021) 4970.
6. B. P. Abbott, LIGO Scientific Collaboration and Virgo Collaboration, *Phys. Rev. Lett.* **116** (February 2016) 061102.
7. D. R. Lorimer and M. Kramer, *Handbook of Pulsar Astronomy* (Cambridge University Press, Cambridge, England, 2005).
8. T. Damour and J. H. Taylor, *Phys. Rev. D* **45** (1992) 1840.
9. M. Kramer, *ApJ* **509** (1998) 856.
10. B. B. P. Perera, M. A. McLaughlin, M. Kramer, I. H. Stairs, R. D. Ferdman, et al., *ApJ* **721** (October 2010) 1193.
11. T. Damour and N. Deruelle, *Ann. Inst. H. Poincaré (Physique Théorique)* **43** (1985) 107.
12. T. Damour and N. Deruelle, *Ann. Inst. H. Poincaré (Physique Théorique)* **44** (1986) 263.
13. M. Burgay, N. D'Amico, A. Possenti, R. N. Manchester, A. G. Lyne, et al., *Nature* **426** (December 2003) 531.
14. A. G. Lyne, M. Burgay, M. Kramer, A. Possenti, R. N. Manchester, et al., *Science* **303** (2004) 1153.
15. M. Kramer, I. H. Stairs, R. N. Manchester, N. Wex, A. Deller, W. Coles and et al., *Physical Reviews X* **in press** (December 2021).
16. L. L. Smarr and R. Blandford, *ApJ* **207** (1976) 574.
17. J. M. Weisberg and Y. Huang, *ApJ* **829** (September 2016) 55.
18. LIGO Scientific Collaboration, Virgo Collaboration, et al., *Phys. Rev. Lett.* **119** (October 2017) 161101.
19. J. M. Lattimer, *Universe* **5** (June 2019) 159.
20. G. Boerner, J. Ehlers and E. Rudolph, *A&A* **44** (1975) 417.
21. T. Damour and R. Ruffini, *Academie des Sciences Paris Comptes Rendus Ser. Scie. Math.* **279** (1974) 971.
22. R. A. Hulse and J. H. Taylor, *ApJ* **195** (1975) L51.
23. B. M. Barker and R. F. O'Connell, *ApJ* **199** (1975) L25.
24. V. Radhakrishnan and D. J. Cooke, *Astrophys. Lett.* **3** (1969) 225.
25. J. M. Weisberg, R. W. Romani and J. H. Taylor, *ApJ* **347** (1989) 1030.
26. Z. Arzoumanian, Radio observations of binary pulsars: Clues to binary evolution and tests of general relativity, PhD thesis, Princeton University (1995).
27. I. H. Stairs, S. E. Thorsett, J. H. Taylor and Z. Arzoumanian, Geodetic precession in PSR B1534+12, in *Pulsar Astronomy - 2000 and Beyond, IAU Colloquium 177*, eds. M. Kramer, N. Wex and R. Wielebinski (Astronomical Society of the Pacific, San Francisco, 2000), pp. 121–124.
28. R. N. Manchester, M. Kramer, A. Possenti, A. G. Lyne, M. Burgay, et al., *ApJ* **621** (March 2005) L49.
29. R. D. Ferdman, I. H. Stairs, M. Kramer, R. P. Breton, M. A. McLaughlin, et al., *ApJ* **767** (April 2013) 85.
30. M. Burgay, A. Possenti, R. N. Manchester, M. Kramer, M. A. McLaughlin, et al., *ApJ* **624** (May 2005) L113.
31. A. Noutsos, G. Desvignes, M. Kramer, N. Wex, P. C. C. Freire, et al., *A&A* **643** (November 2020) A143.
32. R. P. Breton, V. M. Kaspi, M. Kramer, M. A. McLaughlin, M. Lyutikov, et al., *Science* **321** (July 2008) 104.

33. M. Lyutikov and C. Thompson, *ApJ* **634** (December 2005) 1223.
34. M. Kramer and I. H. Stairs, *Ann. Rev. Astr. Ap.* **46** (September 2008) 541.
35. M. Kramer and N. Wex, *Class. Quant Grav.* **26** (April 2009) 073001.
36. G. Desvignes, M. Kramer, K. Lee, J. van Leeuwen, I. Stairs, et al, *Science* **365** (September 2019) 1013.
37. S. E. Gralla, A. Lupsasca and A. Philippov, *apj* **851** (December 2017) 137.
38. R. Yuen and D. B. Melrose, *PASA* **31** (October 2014) e039.
39. Y. Gupta and R. T. Gangadhara, *ApJ* **584** (2003) 418.
40. S. Johnston and M. Kramer, *MNRAS* **490** (December 2019) 4565.
41. M. Kramer, *International Journal of Modern Physics D* **23** (December 2014) 1430004.
42. A. D. Cameron, D. J. Champion, M. Kramer, M. Bailes, E. D. Barr, et al., *MNRAS* **475** (March 2018) L57.
43. M. Kramer, I. H. Stairs, V. Venkatraman Krishnan, P. C. C. Freire, F. Abbate, et al., *MNRAS* **504** (June 2021) 2094.
44. L. Shao and N. Wex, *Science China Physics, Mechanics, and Astronomy* **59** (September 2016) 699501.
45. N. Wex and M. Kramer, *Universe* **6** (September 2020) 156.
46. J. G. Williams, S. G. Turyshev and D. H. Boggs, *International Journal of Modern Physics D* **18** (January 2009) 1129.
47. F. Hofmann and J. Müller, *Classical and Quantum Gravity* **35** (February 2018) 035015.
48. T. Damour and G. Schäfer, *Phys. Rev. Lett.* **66** (1991) 2549.
49. S. M. Ransom, I. H. Stairs, A. M. Archibald, J. W. T. Hessels, D. L. Kaplan, et al., *Nature* **505** (January 2014) 520.
50. P. C. C. Freire, M. Kramer and N. Wex, *Classical and Quantum Gravity* **29** (September 2012) 184007.
51. A. M. Archibald, N. V. Gusinskaia, J. W. T. Hessels, A. T. Deller, D. L. Kaplan, et al., *Nature* **559** (2018) 73.
52. G. Voisin, I. Cognard, P. C. C. Freire, N. Wex, L. Guillemot, G. Desvignes, M. Kramer and G. Theureau, *A&A* **638** (June 2020) A24.
53. L. Shao, N. Wex and M. Kramer, *Phys. Rev. Lett.* **120** (June 2018) 241104.
54. J. D. Bekenstein, *Phys. Rev. D* **70** (October 2004) 083509.
55. S. Boran, S. Desai, E. O. Kahya and R. P. Woodard, *Physical Reviews D* **97** (February 2018) 041501.
56. T. Damour and G. Esposito-Farese, *Phys. Rev. Lett.* **70** (1993) 2220.
57. T. Damour and G. Esposito-Farese, *Phys. Rev. D* **54** (1996) 1474.
58. C. M. Will, *Living Reviews in Relativity*, **17** (2014), 4.